Electromagnetic radiation as a probe of the initial state and of viscous dynamics in relativistic nuclear collisions

Gojko Vujanovic, Jean-François Paquet, Gabriel S. Denicol, Matthew Luzum, Sangyong Jeon, and Charles Gale

Phys. Rev. C **94**, 014904 — Published 8 July 2016

DOI: 10.1103/PhysRevC.94.014904

Electromagnetic radiation as a probe of the initial state and of viscous dynamics in relativistic nuclear collisions

Gojko Vujanovic,[1,2] Jean-François Paquet,[1,3] Gabriel S. Denicol,[1,4]
Matthew Luzum,[5,6] Sangyong Jeon,[1] and Charles Gale[1]

[1]*Department of Physics, McGill University, 3600 rue University, Montréal, Québec H3A 2T8, Canada*
[2]*Department of Physics, Ohio State University, 191 West Woodruff Avenue, Columbus, Ohio 43210, USA*
[3]*Department of Physics & Astronomy, Stony Brook University, Stony Brook, New York 11794, USA*
[4]*Physics Department, Brookhaven National Lab, Building 510A, Upton, New York 11973, USA*
[5]*Departamento de Física de Partículas and IGFAE,*
Universidade de Santiago de Compostela, E-15706 Santiago de Compostela, Galicia-Spain
[6]*Instituto de Física - Universidade de São Paulo, Rua do Matão Travessa R,*
no. 187, 05508-090, Cidade Universitária, São Paulo, Brasil

The penetrating nature of electromagnetic signals makes them suitable probes to explore the properties of the strongly-interacting medium created in relativistic nuclear collisions. We examine the effects of the initial conditions and shear relaxation time on the spectra and flow coefficients of electromagnetic probes, using an event-by-event 3+1D viscous hydrodynamic simulation (MUSIC).

PACS numbers: 12.38.Mh, 47.75.+f, 25.75.Cj

I. INTRODUCTION

Ultra-relativistic heavy-ion collisions at the Relativistic Heavy Ion Collider (RHIC) and the Large Hadron Collider (LHC) are able to reach temperatures high enough to create and study the quark-gluon plasma (QGP) in a controlled experimental environment. Experiments performed at these colliders showed that this new state of matter can be well described by relativistic hydrodynamics [1, 2].

Investigating and extracting the properties of the QGP from heavy-ion collisions is not a simple task since this phase of matter is only created for a small period of time. Currently, most of our knowledge of the properties of this hot QCD medium originates from analyzing the momentum distribution of hadrons. However, the information that can be extracted from hadrons is limited, since such particles are emitted mainly at the very late stages of the collision. Indeed, hydrodynamical studies at RHIC energies have shown that such probes are poorly sensitive to several properties of the thermalized QCD fluid, such as the initial values of the shear-stress tensor [3], the temperature dependence of the shear viscosity coefficient [4], and the dependence on the relaxation time [5], among others.

On the other hand, since photons and dileptons are emitted throughout the entire evolution of the medium, including the QGP sector, they are expected to carry information about the early stages of the collision and can potentially be used as probes of the fluid's transport properties. The PHENIX Collaboration was the first to release measurements of the direct photon elliptic flow [6], soon followed by the ALICE Collaboration, which released preliminary measurements of the same observable at LHC energies [7]. The main feature observed by both collaborations is the significant yield of direct photons and their large azimuthal momentum anisotropy.

Whether hydrodynamical models can be adapted to describe the photon v_2 is still under investigation. Early hydrodynamical calculations under-predicted the elliptic flow by factors of $\sim 2-4$ [8–10]. Recent calculations using more complete hadronic photon emission rates and improved modeling of the medium show a significantly reduced tension between theoretically computed elliptic flow and the measured v_2 both at RHIC and the LHC [11, 12]. As far as the dilepton yield is concerned, theoretical models were able to quantitatively describe the data from the SPS and RHIC (see [13, 14] for a review). At the time of this writing, the dielectron elliptic flow had only been measured by the STAR Collaboration [15], and current theoretical calculations are consistent with data [16], though large uncertainties are preventing more definitive conclusions.

In this paper we investigate how electromagnetic probes can complement hadronic probes in understanding the non-equilibrium dynamics of the hot QCD in the early stages of the collision. We explicitly demonstrate that thermal photons and dileptons emitted by the QGP are sensitive to the shear relaxation time — a transport coefficient that has a negligible effect on hadronic observables. We further study the effects that a non-equilibrium initial condition can have on EM probes. Thermal photons and dileptons are found to be affected by the non-equilibrium aspects of the initial profile.

II. MODELING THE EVOLUTION OF THE MEDIUM CREATED AT RHIC

A. Initial condition

The hydrodynamical evolution starts at time $\tau_0 = 0.4$ fm with an initial energy density profile given by the Glauber model. In our implementation of this model, the initial energy density profile is assumed to be factorized into a longitudinal part and a transverse part, as originally proposed in Ref. [17]:

$$\varepsilon\left(\tau_0, x, y, \eta_s\right) = \exp\left[-\frac{\left(|\eta_s| - \eta_{\rm flat}/2\right)^2}{2\eta_\sigma^2}\theta\left(|\eta_s| - \eta_{\rm flat}/2\right)\right]\varepsilon_T\left(x, y\right).$$

In the longitudinal η_s-direction, we take a profile that is approximately boost invariant near mid-rapidity and falls like a Gaussian at large rapidities. We set $\eta_{\rm flat} = 5.9$ and $\eta_\sigma = 0.4$. The energy density in the transverse direction is given by the Monte Carlo Glauber (MC Glauber) model

$$\varepsilon_T\left(x, y\right) = W\left[\alpha n_{\rm BC}\left(x, y\right) + \left(1 - \alpha\right) n_{\rm WN}\left(x, y\right)\right],$$

where we defined

$$n_{\rm BC/WN}\left(x, y\right) = \frac{1}{2\pi\sigma^2}\sum_{i=1}^{N_{\rm bin/part}} \exp\left[-\frac{\left(x - x_i\right)^2 + \left(y - y_i\right)^2}{2\sigma^2}\right],$$

with W being an overall normalization factor, and α a parameter dictating the proportion in which wounded nucleons and binary collisions contribute to the energy density profile in the transverse plane. Furthermore, $N_{\rm part}$ and $N_{\rm bin}$ are the number of participants and binary collision of a given event and (x_i,y_i) are the coordinates of the corresponding participant or binary collision on the transverse plane. In this work, we set $W = 6.16$ GeV/fm and $\alpha = 0.25$ for all simulations. The number and coordinates of participants and binary collisions are calculated taking a nucleon-nucleon inelastic cross section of $\sigma_{NN} = 42.1$ mb. The fluctuation scale σ, which specifies the length scale of energy density fluctuations, is taken to be $\sigma = 0.4$ fm. The above parameters are based on Ref. [18], but were adjusted to fit the charged pion transverse momentum spectrum and charged hadron elliptic flow at $\sqrt{s_{NN}} = 200$ GeV at RHIC in the 20%–40% centrality class.

We select the centrality class by sampling events in a certain range of impact parameters. For the 20%–40% centrality class considered in this paper, we sampled events with impact parameters, $b_{\rm imp}$, ranging from $b_{\rm imp} = 6.7$–9.48 fm. A total of two hundred events were sampled.

Finally, we provide initial conditions for the 4-velocity, u^μ, and shear-stress tensor, $\pi^{\mu\nu}$. The initial flow profile is set to be zero, i.e., $u_0^\tau = 1$, $u_0^x = 0$, $u_0^y = 0$, and $u_0^{\eta_s} = 0$, while the initial shear-stress tensor is always assumed to be proportional to its corresponding Navier-Stokes value,

$$\pi^{\mu\nu}(\tau_0) = c \times {\rm diag}\left(0, \frac{2\eta}{3\tau_0}, \frac{2\eta}{3\tau_0}, -\frac{4\eta}{3\tau_0}\right),$$

where the parameter c is a constant and will be varied between 0 and 1 in this work, and η is the effective shear viscosity coefficient discussed in the next section.

B. Relativistic dissipative fluid dynamics

The time evolution of the system is described using relativistic dissipative fluid dynamics. The evolution of the energy-momentum tensor $T^{\mu\nu}$ is first constrained by the conservation law:

$$\partial_\mu T^{\mu\nu} = 0, \tag{1}$$

where $T^{\mu\nu} = \varepsilon u^\mu u^\nu - \Delta^{\mu\nu} P + \pi^{\mu\nu}$ with P being the thermodynamic pressure and $\Delta^{\mu\nu} = g^{\mu\nu} - u^\mu u^\nu$ the projection operator onto the 3-space orthogonal to velocity. We employ Landau's definition of the velocity field [19] and assume that bulk viscous pressure and baryon number 4-current are identically zero in all space-time points. The equation of state, which dictates how the thermodynamic pressure changes as a function of energy density, is taken from Ref. [20] and corresponds to a parametrization of a lattice QCD calculation, at high temperatures, smoothly connected to a parametrization of the hadron resonance gas at lower temperatures. At temperatures below $T_{\rm ch} = 0.16$ GeV, this

equation of state follows a partial chemical equilibrium prescription, which assumes that ratios of particle multiplicity remain fixed for all $T < T_{\rm ch}$ [17, 21].

The evolution equation for the shear-stress tensor is provided by Israel-Stewart theory [22, 23],

$$\tau_\pi \Delta^{\mu\nu}_{\alpha\beta} u^\lambda \partial_\lambda \pi^{\alpha\beta} + \pi^{\mu\nu} = 2\eta\sigma^{\mu\nu} - \frac{4}{3}\tau_\pi \pi^{\mu\nu}\partial_\lambda u^\lambda, \tag{2}$$

where $\sigma^{\mu\nu} = \Delta^{\mu\nu}_{\alpha\beta}\partial^\alpha u^\beta$ is the shear tensor and $\Delta^{\mu\nu}_{\alpha\beta} = \left(\Delta^\mu_\alpha \Delta^\nu_\beta + \Delta^\mu_\beta \Delta^\nu_\alpha\right)/2 - \left(\Delta_{\alpha\beta}\Delta^{\mu\nu}\right)/3$ is the double, symmetric, traceless projection operator. Above, we introduced two transport coefficients, the shear viscosity coefficient, η, and the shear relaxation time, τ_π. In principle, additional nonlinear terms exist in the Israel-Stewart theory [24, 25], but for the sake of simplicity, they are not included in this work.

The transport coefficients are functions of the temperature (and the net baryon chemical potential, if the net baryon number density is nonzero) that, in principle, should be computed from the underlying microscopic theory. However, reliable calculations of the aforementioned transport coefficients in the strongly coupled regime are not yet possible. In this work, we assume the existence of an effective shear viscosity coefficient that is proportional to the entropy density,

$$\frac{\eta}{s} = 0.08.$$

Meanwhile, the relaxation time is assumed to be of the form,

$$\begin{aligned} \tau_\pi &= b_\pi \frac{\eta}{\varepsilon + P} \\ &= b_\pi \frac{\eta}{s}\frac{1}{T}, \end{aligned} \tag{3}$$

where we have used the Euler relation $\varepsilon + P = sT$ for a system free of conserved charges, such as net baryon number. The variable b_π is being varied from 5 to 20. We note that, in order to preserve causality, the coefficient b_π is constrained to be $b_\pi \geq 4/[3\left(1 - c_s^2\right)]$, where c_s is the velocity of sound [26].

The fluid-dynamical equations are solved numerically using the MUSIC 2.0 simulation code, an updated version of the simulation code presented in Ref. [18, 27, 28]. This simulation code has recently been tested against semi-analytic solutions of Israel-Stewart theory and was shown to provide accurate solutions of such type of equations [29]. The simulations performed in this paper used a time step of $\Delta\tau = 0.03$ fm and a grid spacing of $\Delta x = \Delta y = 1/6$ fm and $\Delta\eta_s = 1/5$. Such values are small enough to ensure that we achieved the continuum limit for the particular observables explored in this study.

C. Particle production

Hadrons are produced using the traditional Cooper-Frye prescription [30], with a constant temperature freeze-out hypersurface of $T_{FO} = 145$ MeV [18], and including all 2– and 3–particle decays of hadronic resonances [31] up to 1.3 GeV.

In the Cooper-Frye formalism, one first needs to specify the local momentum distribution of hadrons. For an ideal hadron resonance gas, these would correspond to Fermi-Dirac or Bose-Einstein distributions, with the appropriate mass and degeneracy factors. For dissipative systems, this is no longer the case and the distribution function should be generalized to also include non-equilibrium corrections. Here, we use [32]

$$f^i_{\mathbf{k}} = f^i_{0\mathbf{k}} + \delta f^i_{\mathbf{k}}; \quad \delta f^i_{\mathbf{k}} = f^i_{0\mathbf{k}}\left(1 + a f^i_{0\mathbf{k}}\right)\frac{\pi^{\mu\nu}}{2\left(\varepsilon + P\right)T^2} k^i_\mu k^i_\nu, \tag{4}$$

where the index i specifies the hadron species, k^i_μ is that hadron's 4–momentum, and $a = 1\,(-1)$ for bosons (fermions). The chemical potentials $\mu^i_{\rm PCE}(T)$ arising from the partial chemical equilibrium prescription are implicitly present throughout this work, both in the Cooper-Frye formalism and in the production rates of electromagnetic radiation, discussed in the next section.

III. PRODUCTION RATES OF ELECTROMAGNETIC PROBES

The production rate of electromagnetic radiation from a QCD plasma is known only in very specific limits of the QCD phase diagram. At low temperatures, the emission rate has been described using effective Lagrangians

with hadronic degrees of freedom [13, 33–35]. For weakly-coupled and high temperature plasma, the rate has been computed perturbatively at next-to-leading order for photons [36] and dileptons [37–39]. Electromagnetic emission rates that take into account deviations from local thermodynamic equilibrium — essential when the emitting medium is a viscous fluid — have been published recently [9, 10, 16, 40, 41], although they have not yet been extended to include next-to-leading order processes.

Since EM rates are known only for the low and high temperature limits of the QCD medium, the approach taken in this paper is to use each rate in their own temperature limits. In the crossover region, here taken to be in the temperature range $T = 184$–220 MeV [20], we use rates that are a linear interpolation of hadronic and QGP rates.

For the strong coupling constant, we used a constant value of $g_s = 2$, corresponding to $\alpha_s \approx 0.32$. The rates used for photons and dileptons are described in more details in the following subsections.

A. Dileptons

The dilepton production rate can be written as

$$\frac{d^4R^{\ell^+\ell^-}}{d^4q} = -\frac{L(M)}{M^2}\frac{\alpha_{EM}^2}{\pi^3}\frac{\mathrm{Im}\Pi_{EM}^R(M,|\mathbf{q}|;T)}{e^{q^0/T}-1}\ ;\ \ L(M) = \left(1+\frac{2m_\ell^2}{M^2}\right)\sqrt{1-\frac{4m_\ell^2}{M^2}}\ , \tag{5}$$

where $M^2 = q_\mu q^\mu$, $q^0 = \sqrt{M^2+|\mathbf{q}|^2}$, and $\mathrm{Im}\Pi_{EM}^R$ is the imaginary part of the retarded virtual photon self-energy.

At low temperatures, we use the Vector meson Dominance Model (VDM), first proposed by Sakurai [42], to relate the real and virtual photon self-energy to hadronic degrees of freedom. According to the VDM, the imaginary part of the retarded photon self-energy $\mathrm{Im}\Pi_{EM}^R$ is related to the imaginary part of the retarded vector meson propagator $\mathrm{Im}D_V^R$ via

$$\mathrm{Im}\Pi_{EM}^R = \sum_{V=\rho,\omega,\phi}\left(\frac{m_V^2}{g_V}\right)^2 \mathrm{Im}D_V^R\ , \tag{6}$$

where $V = \rho, \omega, \phi$ denote the corresponding vector mesons, and g_V is the coupling constant between a vector meson V and a photon. In the Schwinger-Dyson formalism the retarded propagator can be related to the vector meson self energy [43]. The finite temperature piece of the self-energy has been computed through the forward scattering amplitude method first devised by Eletsky *et al.* [34], which includes two contributions: i) resonance scatterings through experimentally observed particles and ii) non-perturbative Regge physics. The vacuum piece of the self-energy is computed using chiral effective Lagrangians. Recently, this method has been extended to include a viscous correction [16] assuming that viscosity modifies the thermal particle distribution according to Eq. (4). The full self-energy can be expressed as $\Pi = \Pi_0 + \delta\Pi$, with $\delta\Pi$ being responsible for the viscous correction to the dilepton rate.

Another approach is to use chiral effective Lagrangians [13] to study the in-medium properties of vector mesons. However, the approach in Ref. [13] has not yet been generalized to a viscous description of the medium, and hence will not be used in this study.

The QGP dilepton emission rate used in this work is calculated from kinetic theory using the Born approximation, since the viscous correction to this rates are known. The rate is given by:

$$\begin{aligned}\frac{d^4R^{\ell^+\ell^-}}{d^4q} &= \int\frac{d^3p_1d^3p_2}{(2\pi)^6E_{\mathbf{p}_1}E_{\mathbf{p}_2}}f_{\mathbf{p}_1}^{(1)}f_{\mathbf{p}_2}^{(2)}\frac{q^2}{2}\sigma\delta^4(q-p_1-p_2)\ ,\\ \sigma &= \frac{16\pi\alpha_{\mathrm{EM}}^2\left(\sum_{q'}e_{q'}^2\right)N_c}{3q^2}\ ,\end{aligned} \tag{7}$$

where σ is the cross section for $q+\bar{q}\to\ell^-+\ell^+$. The QCD number of colors is denoted N_c, and the sum over q' spans over the quark flavors, which we limit to the three lightest: $q' = u, d, s$. Naturally, the single particle momentum distribution functions, $f_{\mathbf{p}}^i$, includes viscous corrections, which we assume to be of the same form as the one shown in Eq. (4). The QGP rate can thus be expressed as:

$$\begin{aligned}\frac{d^4R^{\ell^+\ell^-}}{d^4q} &= \frac{d^4R_0^{\ell^+\ell^-}}{d^4q}+\frac{d^4\delta R^{\ell^+\ell^-}}{d^4q}\\ \frac{d^4\delta R^{\ell^+\ell^-}}{d^4q} &= \frac{q_\mu q_\nu\pi^{\mu\nu}}{2T^2(\varepsilon+P)}b_2(q^0,|\mathbf{q}|;T)\end{aligned} \tag{8}$$

where the expression for $b_2(q^0,|\mathbf{q}|;T)$ can be found in [16, 41].

B. Photons

At low temperatures, we assume that the photon production can be computed by effectively describing the medium as a gas of light mesons [33, 44], via a massive Yang-Mills Lagrangian coupled with the Vector Dominance Model[1]. In this case, thermal photon production can be computed within a kinetic description:

$$k\frac{d^3R^\gamma}{d^3\mathbf{k}} = \int \frac{d^3p_1}{2E_{\mathbf{p}_1}(2\pi)^3}\frac{d^3p_2}{2E_{\mathbf{p}_2}(2\pi)^3}\frac{d^3p_3}{2E_{\mathbf{p}_3}(2\pi)^3}\frac{1}{2(2\pi)^3} \times(2\pi)^4\delta^{(4)}(P_1+P_2-P_3-K)\left|\mathcal{M}\right|^2 f^{(1)}_{\mathbf{p}_1}f^{(2)}_{\mathbf{p}_2}\left[1\pm f^{(3)}_{\mathbf{p}_3}\right] . \quad (9)$$

This formula captures the $2\to 2$ photon production process in relativistic kinetic theory, with $\mathcal{M}$ being the zero-temperature matrix element corresponding to the photon emission process. Contributions due to photon absorption by the medium are neglected. Some particle decays ($1\to 3$ processes), are included as well in our calculation, with Eq. (9) modified accordingly for such process. The deviation from local equilibrium is taken into account through the presence of $\delta f^i_{\mathbf{p}}$, as in Eq. (4), in the hadron momentum distribution functions $f^i_{\mathbf{p}}$ [9].

At high temperatures, we use the photon emission rate of a weakly-interacting QGP. We use the full leading order rate as computed in [45], which include photon production through Compton scattering, quark-antiquark annihilation and soft bremsstrahlung. For the first two processes, we further include the correction due to the anisotropic momentum distribution associated with the use of viscous hydrodynamics [10].

For both the QGP and hadron gas, the emission rates can be written in the form

$$k\frac{d^3R^\gamma}{d^3\mathbf{k}} = k\frac{d^3R^\gamma_0}{d^3\mathbf{k}} + k\frac{d^3\delta R^\gamma}{d^3\mathbf{k}} \quad (10)$$

which allows for a straightforward separation of the ideal and viscous contributions to the rate, with the viscous correction $\delta R \propto \frac{\pi^{\mu\nu}K_\mu K_\nu}{(\varepsilon+P)}$ given in Ref. [10].

IV. RESULTS AND DISCUSSION

A. Effect of the shear relaxation time on EM probes

In this section we investigate the effect of the shear relaxation time τ_π on EM probes. The effects of τ_π are studied using the parametrization of the relaxation time given by Eq. (3). Different relaxation times are modeled through the parameter b_π, which here is chosen to have three possible values $b_\pi = 5, 10, 20$. The value $b_\pi = 5$ has been obtained in kinetic theory [25]. The initialization of $\pi^{\mu\nu}$ is taken to be $\pi^{\mu\nu}(\tau_0) = 0$. The goal of this section is to compare the sensitivity of electromagnetic probes to τ_π, relative to that of hadronic probes. Indeed, given that EM probes are produced throughout the entire evolution of the medium, they should display a larger sensitivity to the value of b_π, and therefore to the size of τ_π.

We begin by looking at the dimensionless ratio $\bar{\pi}^{\mu\nu} = \pi^{\mu\nu}/(\varepsilon + P)$ in the local rest frame for the three values of τ_π. Averaged over 200 hydrodynamical events for each value of τ_π, $\bar{\pi}^{\mu\nu}$ as a function of $\tau - \tau_0$ is displayed in Fig. 1 for a given transverse position (see caption of Fig. 1 for details). Two important features in this plot, namely the rapid increase of $\bar{\pi}^{\mu\nu}$ for small b_π at early times and the smaller decay rate of $\bar{\pi}^{\mu\nu}$ at late times for large b_π, will have different effects on hadronic and electromagnetic probes. We start by studying the effects of b_π on hadronic emission. In Fig. 2, we show the pion transverse momentum spectra (left panel) and the elliptic flow of charged hadrons (right panel) for our three choices of relaxation time[2]. We can see that changes in the relaxation time have little effect on these observables. This is consistent with the small differences seen in $\bar{\pi}^{\mu\nu}$ at late times. In Fig. 3, we show the spectra and elliptic flow for thermal photons, where the elliptic flow is sensitive to the differences in the evolution of $\bar{\pi}^{\mu\nu}$ observed in Fig. 1. We computed the photon elliptic flow using the scalar product method:

$$v_n^\gamma = \frac{\left\langle v_n^h v_n^\gamma \cos\left[n\left(\Psi_n^\gamma - \Psi_n^h\right)\right]\right\rangle_{\rm ev}}{\sqrt{\left\langle (v_n^h)^2\right\rangle_{\rm ev}}} \quad (11)$$

---

[1] The contribution from baryons and $\pi\pi$ bremsstrahlung, which are known to be significant (see e.g. Ref. [12]), are not included since viscous $\delta f_{\mathbf{p}}$ corrections are not yet known for these rates.

[2] The v_2 of charged hadrons is always computed using the root mean square value of the v_2 computed in each of the 200 hydrodynamical simulations.

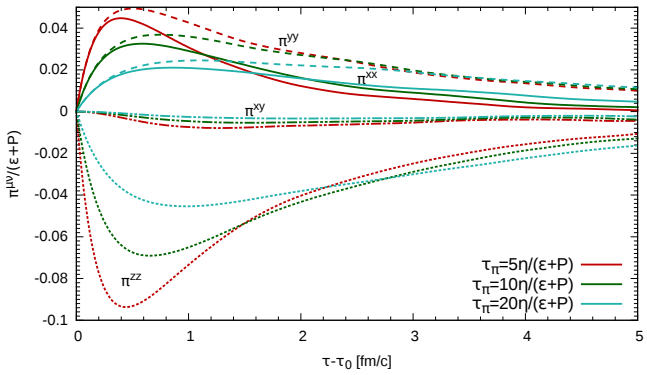

FIG. 1: (Color online) Event averaged shear-stress tensor for $b_\pi = 5, 10, 20$ in the local rest frame of the fluid cell located at x=y=2.67 fm, z=0 fm. Results with $b_\pi = 5$ are in red, $b_\pi = 10$ in dark green and $b_\pi = 20$ in light green. Different types of lines are used for various components of $\pi^{\mu\nu}$. The full line is reserved for π^{xx}, dashed line for π^{yy}, dotted line for π^{zz} and dash-dotted line is used for π^{xy}.

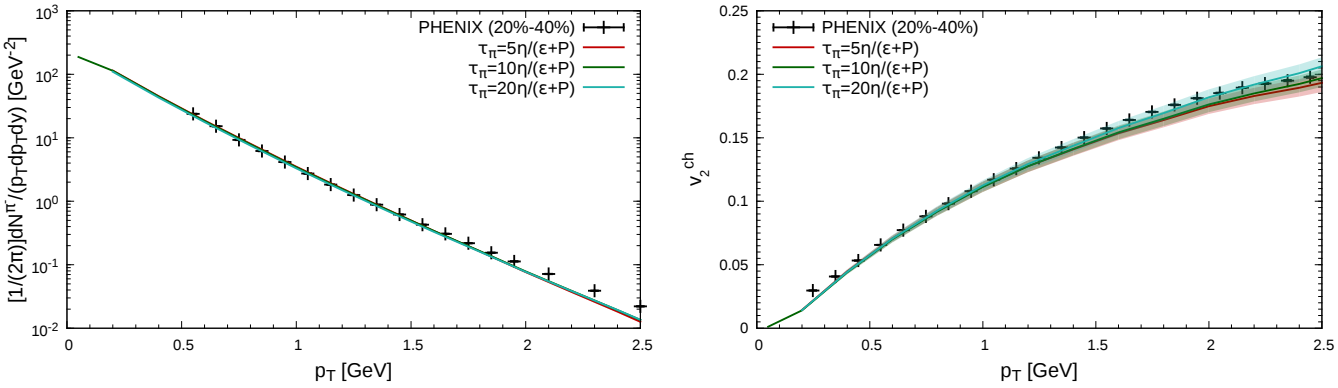

FIG. 2: (Color online) Pion transverse momentum spectra (left panel) and charged hadron differential elliptic flow (right panel) as a function of transverse momentum, for different values of shear relaxation time. Here, and in all subsequent figures of this paper, the colored bands represent the statistical uncertainty associated with 200 hydrodynamical events.

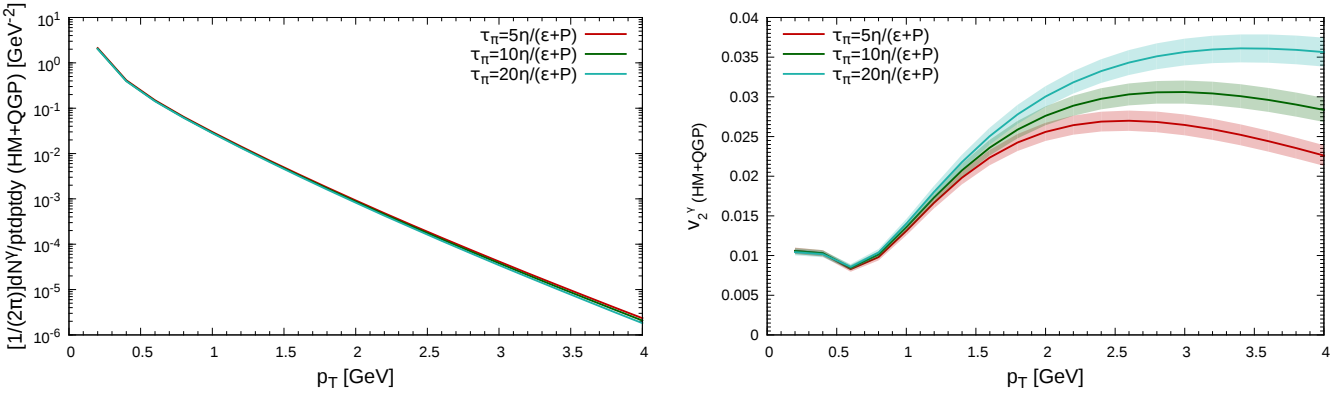

FIG. 3: (Color online) Transverse momentum spectra (left panel) and differential elliptic flow (right panel) of thermal photons as a function of transverse momentum, for different values of shear relaxation time.

where $\langle \ldots \rangle_{\rm ev}$ is an average over events. The v_n^s and Ψ_n^s in single event are given by

$$v_n^s e^{in\Psi_n^s} = \frac{\int dp_T dy d\phi p_T \left[p^0 \frac{d^3N^s}{d^3p}\right] e^{in\phi}}{\int dp_T dy d\phi p_T \left[p^0 \frac{d^3N^s}{d^3p}\right]} \tag{12}$$

where $p^0 d^3N^s/d^3p$ is the single-particle distribution of particle species s. The hadronic v_n^h and Ψ_n^h used in Eq. (11) are integrated over $-0.35 < \eta < 0.35$ and $0.035 < p_T < 3$ GeV to simulate the large bin used experimentally. The photon v_n^γ and Ψ_n^γ are evaluated at mid-rapidity, for given values of p_T. The dilepton anisotropies are computed using the same approach, with the more general single-particle distribution d^4N^s/d^4p.

The photon yield is slightly reduced when increasing b_π from 5 to 20. We have verified that the source of this change originates from a reduction of the viscous correction (δR) to the photon production rate, which is proportional to $\bar{\pi}^{\mu\nu}$ and thus decreases as τ_π increases, as seen in Fig. 1.

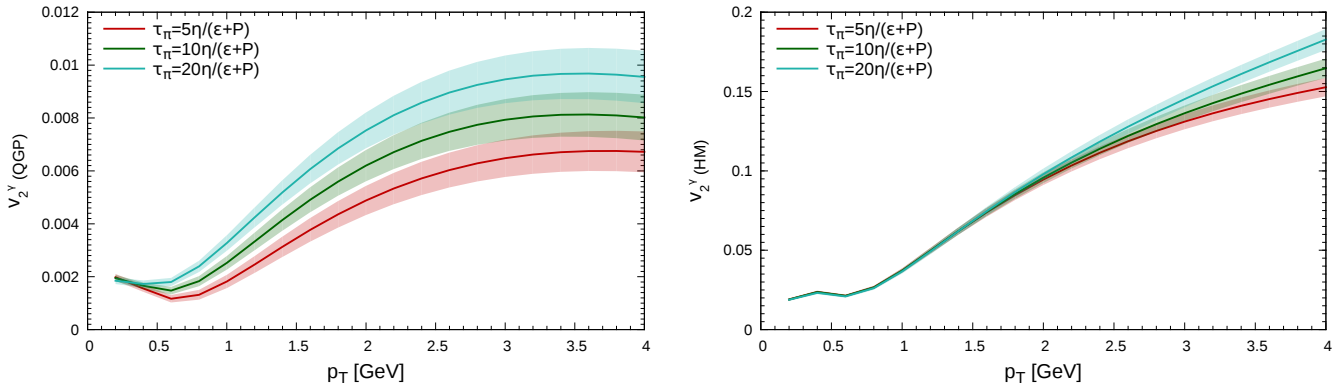

FIG. 4: (Color online) Differential elliptic flow of thermal photons emitted by the QGP (left panel) and emitted by the hadronic medium (HM) (right panel) as a function of transverse momentum, for different values of shear relaxation time.

On the other hand the elliptic flow of photons is increased by more than 50% for $p_T > 3$ GeV. The contribution from the individual sources is isolated in Fig. 4, where the elliptic flow of thermal photons produced in the QGP is in the left panel while the one originating from photons produced in the hadronic medium (HM) is in the right panel. The elliptic flow of thermal photons emitted in the hadronic stage of the evolution is not significantly affected by the relaxation time, while the elliptic flow originating from the QGP thermal photons displays a large dependence on τ_π. Such strong dependence on the relaxation time remains in the total thermal photon v_2 for $p_T \gtrsim 1.5$ GeV, since the total v_2 is a delicate balance — a yield weighted average — of the individual sources.

Therefore, the overall dependence of thermal photons on the relaxation time is not universal, since it depends on a nontrivial balancing between thermal probes emitted at early times (which correspond roughly to QGP emissions) and thermal probes emitted at later times from the HM. In this sense, it is possible that thermal dileptons' invariant mass distribution, integrated over p_T, is better suited to see this behavior. At small invariant masses $M \lesssim 1.1$ GeV, the HM thermal emission dominates. As the invariant mass increases, the relative contribution of QGP dileptons gradually becomes more pronounced, finally dominating at intermediate invariant masses $M \gtrsim 1.1$ GeV. However, the dominance of HM dileptons at low invariant masses is not p_T independent. Hence before describing the invariant mass M distributions of thermal dileptons, let us first consider the p_T distribution at fixed M.

The differential elliptic flow of thermal dileptons $v_2(p_T)$ in the left panel of Fig. 5, for a low invariant mass $M = m_\rho$ — where HM dileptons dominate — is affected by τ_π in manner similar to thermal photon's $v_2(p_T)$ (see right panel of Fig. 3). The flow of intermediate mass dileptons in the right panel of Fig. 5, where QGP emission is the main source, has an increased sensitivity to τ_π; consistent with the left panel of Fig. 4. The effect of τ_π is not limited to $v_2(p_T)$ and is also affecting higher flow harmonics in a similar fashion, as can be seen Fig. 6.

In the left and right panels of Fig. 7, we show the elliptic flow of dileptons emitted from the QGP and HM, respectively, as a function of the dilepton invariant mass. We see that the elliptic flow of dileptons emitted from the QGP increases with τ_π while the opposite behavior is seen for dileptons from the HM. This effect can be better

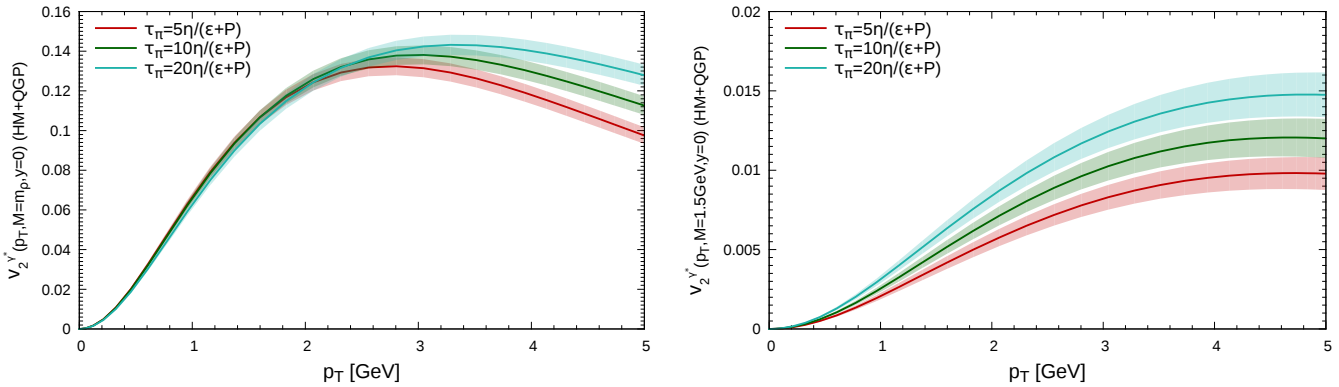

FIG. 5: (Color online) Differential elliptic flow of thermal dileptons for $M = m_\rho$ (left panel) and $M = 1.5$GeV (right panel) as a function of transverse momentum, for different values of shear relaxation time.

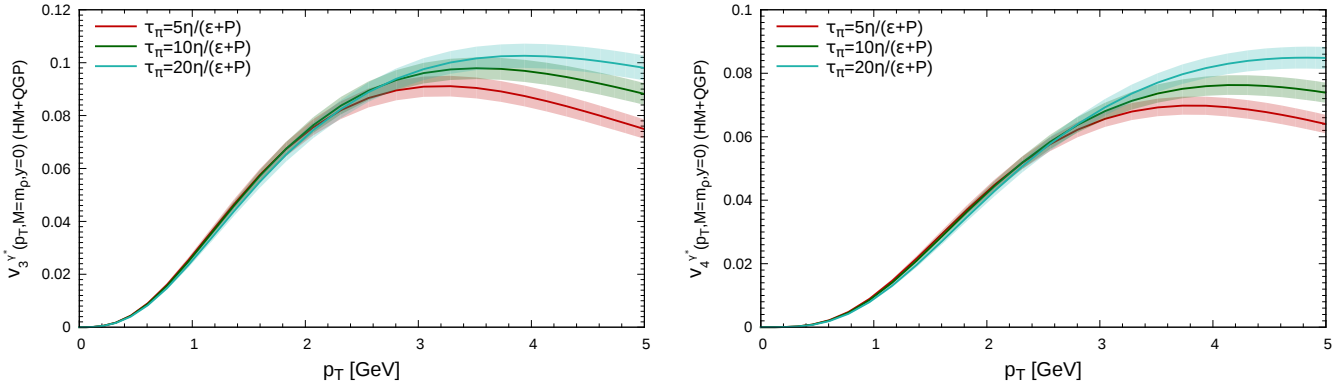

FIG. 6: (Color online) Influence of τ_π on higher flow harmonics of thermal dileptons at $M = m_\rho$: $v_3(p_T)$ is in the left panel, and $v_4(p_T)$ is in the right panel.

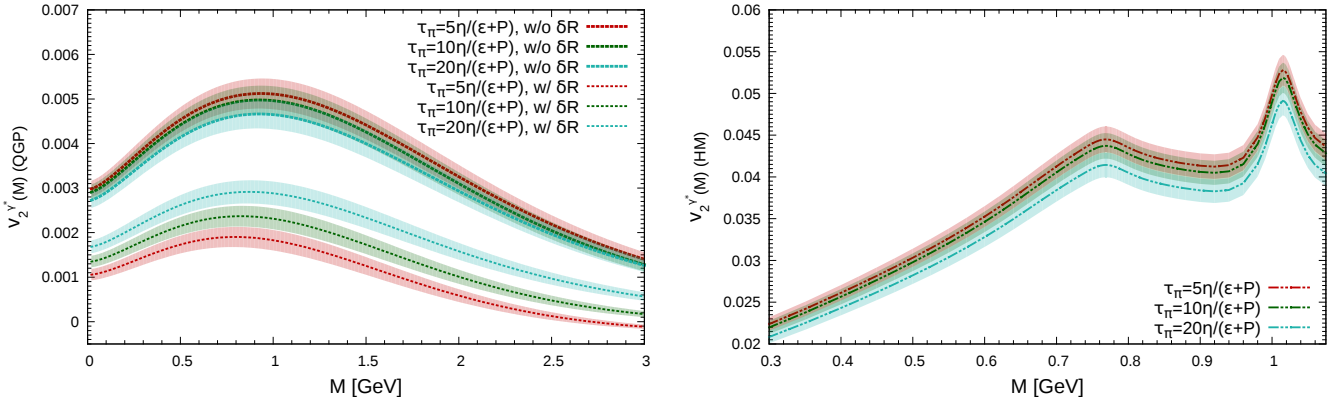

FIG. 7: (Color online) Differential elliptic flow of dileptons emitted by the QGP (left panel) and emitted by the hadronic medium (right panel) as a function of the dilepton invariant mass, for different values of shear relaxation time. The effect of the viscous correction to the QGP rate is presented in the left panel, whereas that of the HM rate is small and hence only results using the rate including the viscous correction is presented in the right panel.

understood by first analyzing the elliptic flow without any viscous corrections to the rates, δR, shown in Fig. 7[3]. In the case without δR corrections, we see that the v_2 of dileptons from both the QGP and HM actually decreases with increasing relaxation time. This happens because, at early times, the shear stress-tensor increases the transverse pressure, leading to a larger anisotropic flow. Since systems with smaller relaxation time develop larger values of shear stress tensor at earlier times (see Fig. 1), they will also have larger values of elliptic flow. On the other hand, the viscous correction to the rate reduces the elliptic flow and is proportional to the shear-stress tensor. Therefore, smaller relaxation times will generate a larger reduction of elliptic flow due to δR. This effect is very large in the QGP and ends up inverting the previously observed trend.

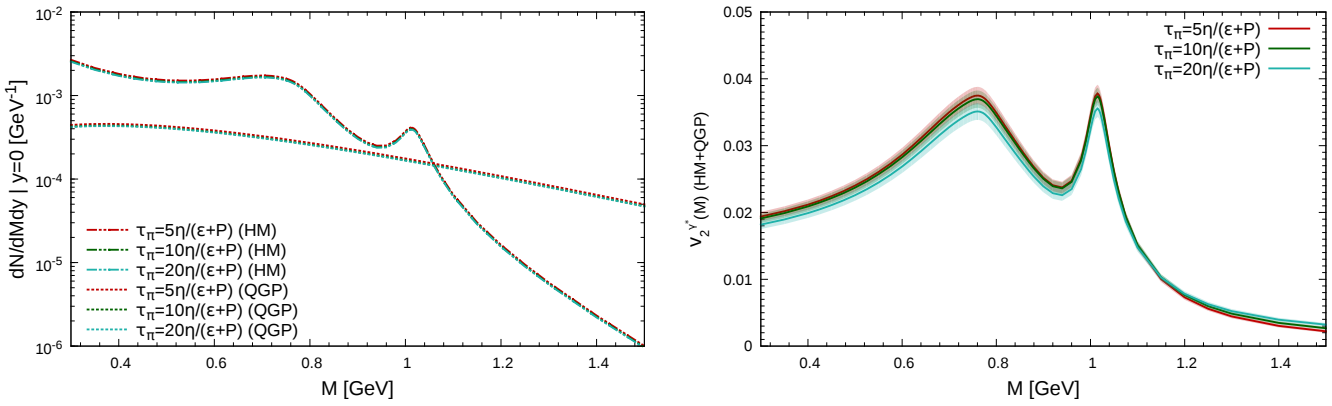

FIG. 8: (Color online) Dilepton yield (left panel) and elliptic flow (right panel) as a function of invariant mass, for different values of shear relaxation time.

Lastly, in Fig. 8 we show the total (QGP+HM) thermal dilepton yield and elliptic flow as a function of invariant mass, for the three different shear relaxation times. At small invariant masses, $M < 1.1$ GeV, the HM dileptons are dominant and we see that the elliptic flow is reduced as the relaxation time increases. On the other hand, for larger invariant masses, $M > 1.1$ GeV, the QGP contribution starts to dominate and the dependence on the relaxation time is inverted. This behavior is expected and is in agreement with the one observed for thermal photons. Note that the invariant mass over which this behavior switches (here, $M \approx 1.1$ GeV) is not universal and depends on other parameters, such as the freeze-out temperature and the initialization time. If one starts the simulation earlier, more QGP thermal photons/dileptons can be emitted, while if one decreases the freeze-out temperature, more hadron gas photons/dileptons are emitted. In fact, because of the initial and freeze-out conditions chosen in this study, the net effect of τ_π on the total thermal $v_2(M)$ is not large as there are incomplete cancellations between the behavior in the QGP and HM sectors. So, one should always take into account the initial and freeze-out conditions when interpreting results of thermal EM emissions in heavy-ion collision simulations.

B. Effect of an initial shear-stress tensor

We explore in this section the sensitivity of EM probes to the presence of a non-vanishing initial shear-stress tensor. As already stated, we use a rescaled Navier-Stokes value of $\pi^{\mu\nu}$ as initial condition:

$$\pi^{\mu\nu}(\tau_0) = c \times \mathrm{diag}\left(0, \frac{2\eta}{3\tau_0}, \frac{2\eta}{3\tau_0}, -\frac{4\eta}{3\tau_0}\right).$$

We use three different values of $c = 0$, $1/2$, 1, with the case $c = 1$ corresponding to the Navier-Stokes limit, $c = 0$ to the equilibrium limit, and $c = 1/2$ to an intermediary case. We set $\tau_\pi = 5\eta/(\varepsilon + P)$ for this whole section, and generate 200 hydrodynamical events for each value of c.

We show in Fig. 9 the time dependence of various components of $\bar{\pi}^{\mu\nu}$, in the rest frame of the fluid, for our three different choices of initial conditions. Notice that differences in $\bar{\pi}^{\mu\nu}$ at early times are washed out within ∼1.5 fm/c, which is about a quarter of the medium's lifetime depicted in Fig. 9. This implies that hadrons should be largely

[3] Though the effect of the viscous correction is negligible on the $v_2(M)$ of HM dileptons, it is included in the right panel of Fig. 7.

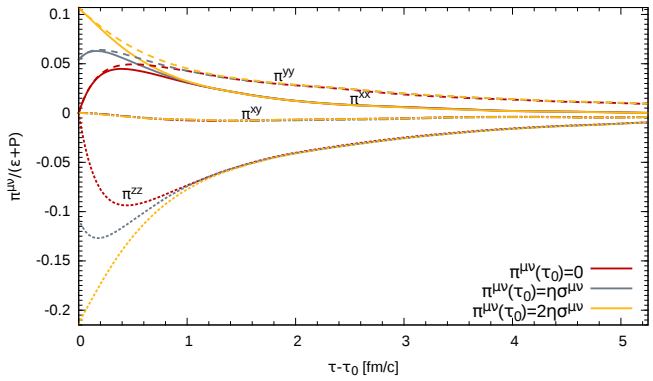

FIG. 9: (Color online) Shear-stress tensor for $c = 0, 1/2, 1$ in the local rest frame of the fluid cell located at x=y=2.$\bar{6}$7 fm, z=0 fm, averaged over all events. Results with $c = 0$ are displayed in red, $c = 1/2$ in gray, and $c = 1$ in yellow.

insensitive to changes in the initial $\bar{\pi}^{\mu\nu}$, though photons and dileptons produced early enough in the collision could be sensitive to the different initial conditions. The spectra and v_2 of hadrons (Fig. 10) agrees with our interpretation of Fig. 9, with both observables showing a very weak dependence on the initial $\pi^{\mu\nu}$.

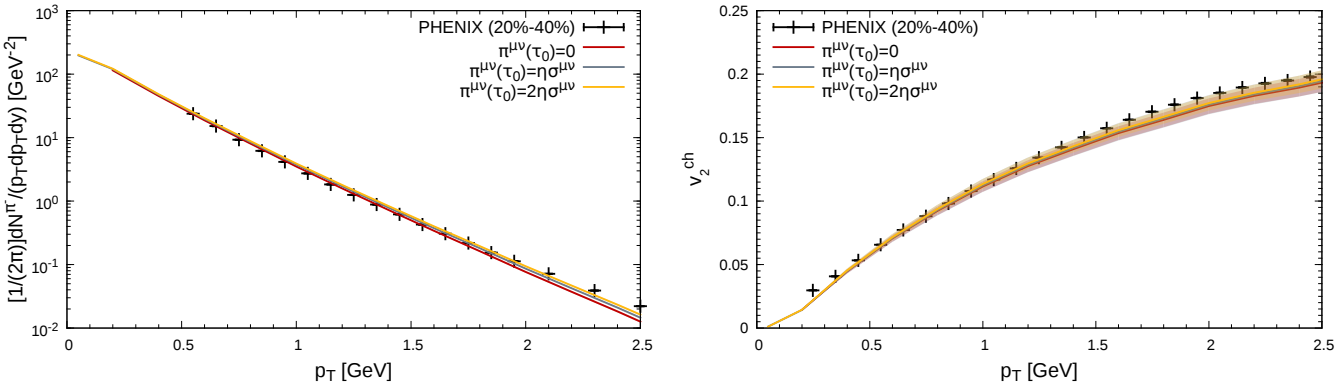

FIG. 10: (Color online) Pion transverse momentum spectra (left panel) and charged hadron differential elliptic flow (right panel) as a function of transverse momentum, for different values of the initial shear-stress tensor.

The photon spectra and v_2 are shown in the left and right panels of Fig. 11, respectively. Similar to what was seen on hadrons, the effect of the initial $\pi^{\mu\nu}$ on the photon spectra is small. However, initial $\pi^{\mu\nu}$ does change the shape of photon v_2; a small increase at low p_T is observed, while the reverse behavior occurs at high p_T.

To better understand the origin of these features, we show in Fig. 12 the v_2 of photons with and without the effect of δR to the photon production rate. Recall that the former will only be sensitive to the feedback of initial $\pi^{\mu\nu}$ on the temperature and flow profiles, while the latter contains the direct effect of the change in $\pi^{\mu\nu}$ on the photon production rate. Indeed, the effect of the initial $\pi^{\mu\nu}$ on the hydrodynamical evolution is not small, and alone produces a significant increase on the photon v_2 (see Fig. 12). The change of behavior seen at high p_T is thus solely due to the effect of the viscous δR correction to the photon production rate. It is more apparent at high p_T because the viscous correction to the rate is larger in that region, relative to low p_T.

The p_T dependence of dilepton's elliptic flow at $M = m_\rho$ is similar to photon's $v_2(p_T)$, as was noted in section IV A, while the $v_2(p_T)$ at higher invariant masses is small. Furthermore, higher flow harmonics of thermal dileptons as a function of p_T at $M = m_\rho$ are also affected in very similar way to v_2. The same statement holds true for higher flow harmonics of thermal photons. Hence, we focus immediately on the thermal dilepton invariant mass distribution.

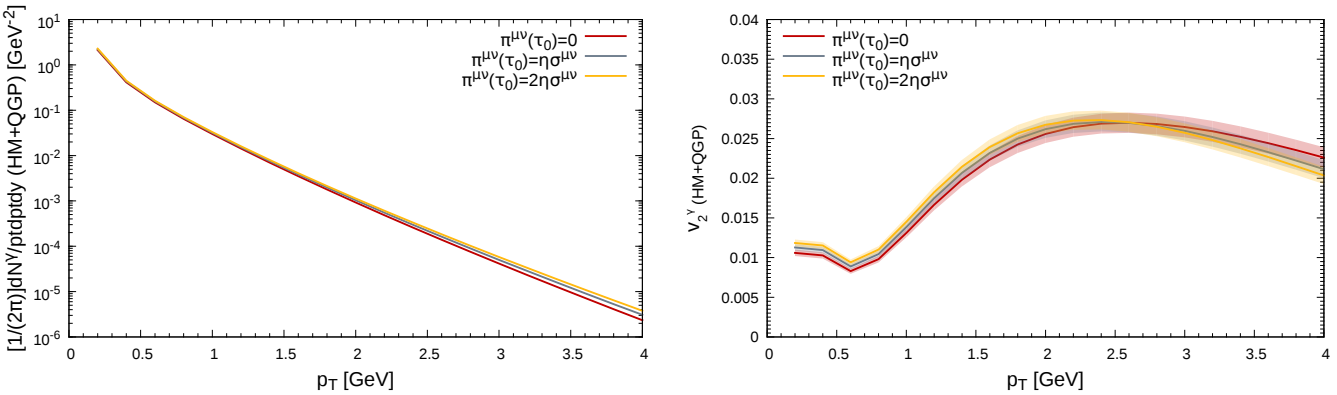

FIG. 11: (Color online) Transverse momentum spectra (left panel) and differential elliptic flow (right panel) of thermal photons as a function of transverse momentum, for different values of initial $\pi^{\mu\nu}$.

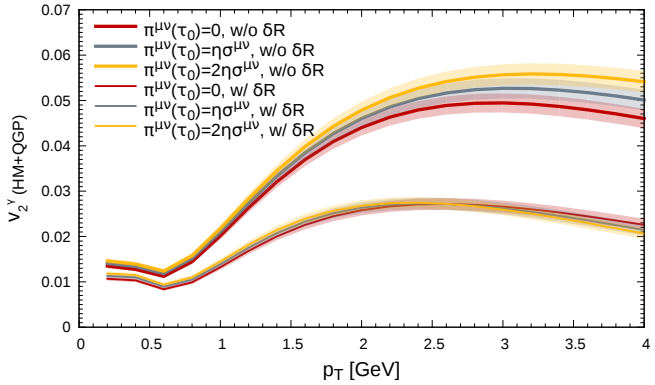

FIG. 12: (Color online) Thermal photon elliptic flow with and without viscous corrections (δR) to the emission rates.

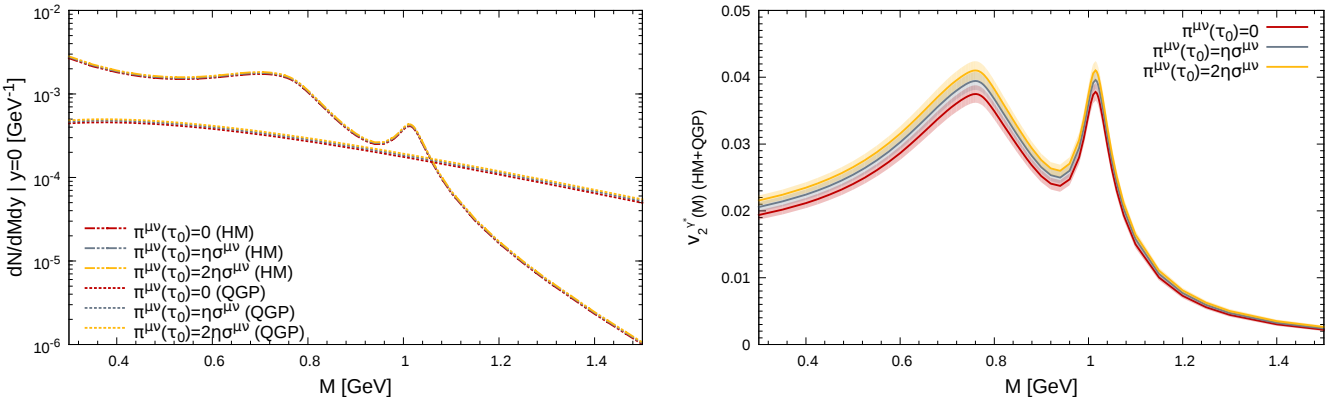

FIG. 13: (Color online) Dilepton yield (left panel) and elliptic flow (right panel) as a function of invariant mass, for different values of initial $\pi^{\mu\nu}$.

The invariant mass yield of thermal dileptons doesn't depend on any viscous corrections[4] and hence it is only

[4] After performing a tensor decomposition on δR, and integrating over the 3-momentum $\mathbf{q}$, the only tensor that can be constructed is proportional to $u_\mu u_\nu$ which vanishes when contracted with $\pi^{\mu\nu}$. Hence the invariant mass distribution of dilepton yield must be independent of δR.

sensitive to the entropy generation that a non-zero $\pi^{\mu\nu}(\tau_0)$ injects into the system, which is small as can be seen in the left panel of Fig. 13. Also, since the invariant mass yield is unaffected by δR, $v_2(M)$ from both thermal sources behaves in a more monotonic fashion as $\pi^{\mu\nu}(\tau_0)$ increases (see the right panel of Fig. 13).

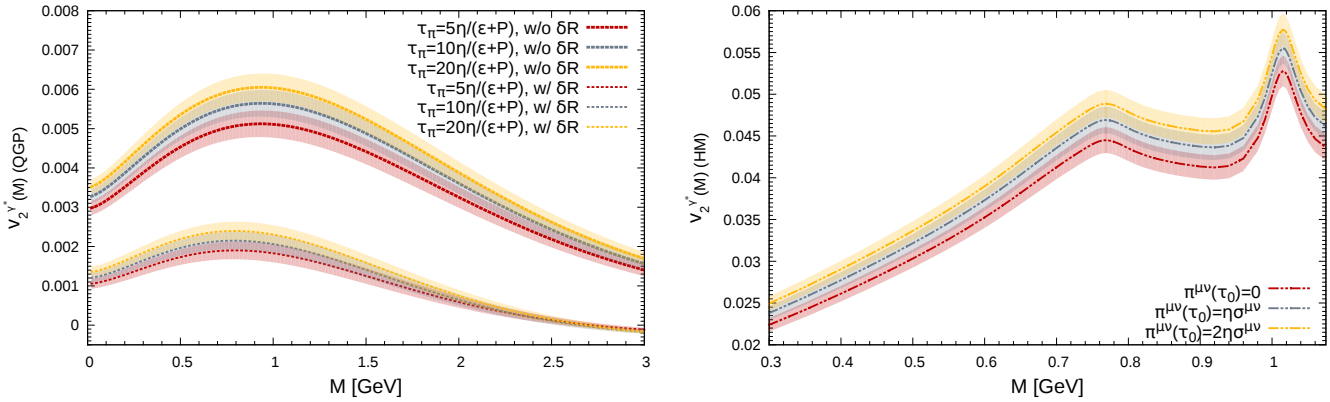

FIG. 14: (Color online) Differential elliptic flow of dileptons emitted by the QGP (left panel) and emitted by the hadronic medium (HM) (see right panel) as a function of the dilepton invariant mass, for different values of initial shear stress tensor. Only the QGP dileptons are calculated with and without viscous correction δR to the rate, while the HM dileptons are calculated with the viscous correction.

Similarly to photon's $v_2(p_T)$ without δR, $v_2(M)$ for the QGP displayed in the left panel of Fig. 14 increases with $\pi^{\mu\nu}(\tau_0)$, while the viscous correction is mostly reducing the v_2. The shape of the $v_2(M)$ changes somewhat at higher M as $\pi^{\mu\nu}(\tau_0)$ increases owing to δR effects in the numerator of v_2, however the viscous correction is not inverting the order of the $v_2(M)$ curves, as was the case for photons. The dilepton HM sector behaves monotonically as a function of M as $\pi^{\mu\nu}(\tau_0)$ increases as shown in the right panel of Fig. 14, receiving an increase of at most $\sim 10\%$ by the time $\pi^{\mu\nu}(\tau_0) = 2\eta\sigma^{\mu\nu}$. Hence, $v_2(M)$ of QGP and HM are directly exposing the modifications of the hydrodynamical evolution, which is seen as a definite trend as far as their sensitivity to $\pi^{\mu\nu}(\tau_0)$ is concerned. In fact, this trend is preserved for dileptons when going to even higher $\pi^{\mu\nu}(\tau_0)$, namely $\pi^{\mu\nu}(\tau_0) = 4\eta\sigma^{\mu\nu}$, while hadrons remain unaffected, as was shown in Ref. [46], where a simpler optical Glauber initial condition was used.

Going back to the Fig. 9, the large pressure gradients in the longitudinal direction are more significantly reduced via a non-zero initial $\bar{\pi}^{zz}(\tau_0)$ — relative to $\bar{\pi}^{zz}(\tau_0) = 0$ — and thus are more efficiently transferred onto the transverse plane. This coupling of the longitudinal and transverse pressure gradients causes an increase in the $v_2(M)$ of QGP dileptons. The elliptic flow $v_2(M)$ of HM dileptons is also increased owing to the fact that a cross-over transition allows for HM dileptons to be emitted from earlier times, where the time evolution of $\bar{\pi}^{\mu\nu}$ is different depending on the value of $\pi^{\mu\nu}(\tau_0)$.

V. CONCLUSIONS

In this paper we studied the effect of the shear relaxation time on thermal photons and dileptons emitted from the QCD medium created at the top RHIC energy. We further analyzed how initial conditions, more specifically initial $\pi^{\mu\nu}(\tau_0)$, of the fluid-dynamical description affect thermal EM probes. We concluded that thermal photons and dileptons can be sensitive to τ_π and to initial conditions of $\pi^{\mu\nu}$ used in the modeling of the collision, while hadronic observables are poorly sensitive to those two parameters.

We have shown that the shear relaxation time has a visible effect on thermal photon and dilepton elliptic flow, with larger values of relaxation time leading to an increase in photon and dilepton $v_2(p_T)$. This indicates that thermal EM probes could be used in the future to provide constraints on the size of the relaxation time for $\pi^{\mu\nu}$ in QCD matter. We further computed higher flow harmonics of thermal dileptons, and have shown that the same effects τ_π induces on v_2 also persist for v_3 and v_4. In addition, we demonstrated that thermal EM radiation is sensitive to the initial conditions of hydrodynamics, specifically the initial shear-stress tensor $\pi^{\mu\nu}(\tau_0)$. In particular, the elliptic flow of thermal dileptons as a function of invariant mass has a definite trend: it increases the elliptic flow with larger $\pi^{\mu\nu}(\tau_0)$.

While larger values of relaxation time and $\pi^{\mu\nu}(\tau_0)$ affect the elliptic flow of thermal photons, the effect is mild except at high transverse momentum, where prompt photons dominate over thermal ones. There is also barely any effect on the thermal photon spectra. In consequence, it does not appear that the effects investigated in this work would

significantly change the agreement with direct photon data of current hydrodynamical calculations (e.g. Ref. [12]). It would nevertheless be interesting to revisit these effects as more realistic initial conditions and more complete viscous corrections to the thermal emission rates become available.

Similarly, the contribution of open heavy flavor hadron pairs, whose semi-leptonic decay contribute to dileptons, needs to be included to the list of dilepton sources. Indeed, it was recently shown that open charm hadrons [16] traveling through the medium develop flow which contributes to dilepton $v_2(M)$ in the intermediate mass region[5]. In the low mass region, late decays of pseudo-scalar mesons and ω and ϕ mesons all contribute to the dilepton "cocktail" production. However, in the invariant mass window $0.6 < M < 0.78$ GeV, thermal dilepton production is the dominant source of lepton pairs [16], and thus results presented here should persist even when the "cocktail" and open heavy flavor contributions are added. A more in-depth study including the "cocktail" and open heavy flavor dileptons is in progress.

After taking into account all these sources, extracting transport coefficients from EM probes will remain a challenging task, but we are optimistic it can be led to a fruitful completion. In the case of dileptons, the task might be made easier if heavy flavor tracking is used to remove the open heavy flavor signal from the measured dilepton flow in the intermediate mass and low mass regions. Performing this subtraction in experimental dilepton data opens an interesting "window" to extract the transport coefficients of QGP in the intermediate mass region. In the low mass region, removing the dilepton "cocktail" will help study transport coefficients coming from a low temperature QCD medium. On the photon side, once good agreement with direct photon measurements is achieved, one interesting avenue to isolate the thermal contribution may lie in taking ratios of anisotropic coefficients, making thermal photons stand out from sources that have small/negligible flow anisotropies [47]. These would all strengthen the capabilities of photons and dileptons as complementary probes of the properties of QCD media, especially of non-equilibrium properties of the initial conditions.

Acknowledgments

We are happy to acknowledge helpful discussions with C. Shen and B. Schenke. This work was supported in part by the Natural Sciences and Engineering Research Council of Canada, and in part by the Director, Office of Energy Research, Office of High Energy and Nuclear Physics, Division of Nuclear Physics, of the U.S. Department of Energy under Contracts No. DE-AC02-98CH10886, DE-AC02-05CH11231, and DE-SC0004286. G. Vujanovic acknowledges support by the Fonds de Recherche du Québec — Nature et les Technologies (FRQNT), the Canadian Institute for Nuclear Physics, and by the Seymour Schulich Scholarship, while G.S. Denicol acknowledges support through a Banting Fellowship from the Government of Canada. Computations were performed on the Guillimin supercomputer at McGill University under the auspices of Calcul Québec and Compute Canada. The operation of Guillimin is funded by the Canada Foundation for Innovation (CFI), the National Science and Engineering Research Council (NSERC), NanoQuébec, and the Fonds de Recherche du Québec — Nature et les Technologies (FRQNT).

[1] U. Heinz and R. Snellings, Ann.Rev.Nucl.Part.Sci. **63**, 123 (2013), [arXiv:nucl-th/1301.2826].
[2] C. Gale, S. Jeon, and B. Schenke, Int.J.Mod.Phys. **A28**, 1340011 (2013), [arXiv:nucl-th/1301.5893].
[3] H. Song and U. W. Heinz, Phys.Rev. **C81**, 024905 (2010), [arXiv:nucl-th/0909.1549].
[4] H. Niemi, G. S. Denicol, P. Huovinen, E. Molnar, and D. H. Rischke, Phys.Rev.Lett. **106**, 212302 (2011), [arXiv:nucl-th/1101.2442].
[5] H. Song and U. W. Heinz, Phys.Rev. **C78**, 024902 (2008), [arXiv:nucl-th/0805.1756].
[6] A. Adare et al. (PHENIX Collaboration), Phys.Rev.Lett. **109**, 122302 (2012), [arXiv:nucl-ex/1105.4126].
[7] D. Lohner (ALICE), J.Phys.Conf.Ser. **446**, 012028 (2013), [arXiv:hep-ex/1212.3995].
[8] R. Chatterjee, H. Holopainen, I. Helenius, T. Renk, and K. J. Eskola, Phys.Rev. **C88**, 034901 (2013), [arXiv:hep-ph/1305.6443].
[9] M. Dion, J.-F. Paquet, B. Schenke, C. Young, S. Jeon, et al., Phys.Rev. **C84**, 064901 (2011), [arXiv:hep-ph/1109.4405].
[10] C. Shen, J.-F. Paquet, U. Heinz, and C. Gale, Phys. Rev. **C91**, 014908 (2015), [arXiv:nucl-th/1410.3404].
[11] H. van Hees, M. He, and R. Rapp, Nucl. Phys. **A933**, 256 (2015), [arXiv:nucl-th/1404.2846].
[12] J.-F. Paquet, C. Shen, G. S. Denicol, M. Luzum, B. Schenke, S. Jeon, and C. Gale (2015), [arXiv:hep-ph/1509.06738].

[5] Drell-Yan processes and the decay of heavy quarkonium also contribute to the total dilepton spectrum. However, in the low and intermediate mass regions, their contribution is usually small enough to be neglected.

[13] R. Rapp and J. Wambach, Adv.Nucl.Phys. **25**, 1 (2000), [arXiv:hep-ph/9909229].
[14] R. Rapp, J. Wambach, and H. van Hees (2009), [arXiv:hep-ph/0901.3289].
[15] L. Adamczyk et al. (STAR Collaboration) (2014), [arXiv:nucl-ex/1402.1791].
[16] G. Vujanovic, C. Young, B. Schenke, R. Rapp, S. Jeon, et al., Phys.Rev. **C89**, 034904 (2014), [arXiv:nucl-th/1312.0676].
[17] T. Hirano and K. Tsuda, Phys.Rev. **C66**, 054905 (2002), [arXiv:nucl-th/0205043].
[18] B. Schenke, S. Jeon, and C. Gale, Phys.Rev. **C85**, 024901 (2012), [arXiv:hep-ph/1109.6289].
[19] L. D. Landau and E. M. Lifshitz, Fluid Mechanics Second Edition: Volume 6 (Course of Theoretical Physics), Butterworth-Heinemann (1987).
[20] P. Huovinen and P. Petreczky, Nucl.Phys. **A837**, 26 (2010), [arXiv:hep-ph/0912.2541].
[21] H. Bebie, P. Gerber, J. Goity, and H. Leutwyler, Nucl.Phys. **B378**, 95 (1992).
[22] W. Israel and J. Stewart, Annals Phys. **118**, 341 (1979).
[23] W. Israel, Annals Phys. **100**, 310 (1976).
[24] G. S. Denicol, T. Koide, and D. H. Rischke, Phys.Rev.Lett. **105**, 162501 (2010), [arXiv:nucl-th/1004.5013].
[25] G. S. Denicol, H. Niemi, E. Molnar, and D. H. Rischke, Phys.Rev. **D85**, 114047 (2012), [arXiv:nucl-th/1202.4551].
[26] S. Pu, T. Koide, and D. H. Rischke, Phys.Rev. **D81**, 114039 (2010), [arXiv:hep-ph/0907.3906].
[27] B. Schenke, S. Jeon, and C. Gale, Phys.Rev. **C 82**, 014903 (2010), [arXiv:hep-ph/1004.1408].
[28] B. Schenke, S. Jeon, and C. Gale, Phys.Rev.Lett. **106**, 042301 (2011), [arXiv:hep-ph/1009.3244].
[29] H. Marrochio, J. Noronha, G. S. Denicol, M. Luzum, S. Jeon, et al. (2013), [arXiv:nucl-th/1307.6130].
[30] F. Cooper and G. Frye, Phys.Rev. **D10**, 186 (1974).
[31] J. Sollfrank, P. Koch, and U. W. Heinz, Z.Phys. **C52**, 593 (1991).
[32] D. Teaney, Phys.Rev. **C68**, 034913 (2003), [arXiv:nucl-th/0301099].
[33] S. Turbide, R. Rapp, and C. Gale, Phys.Rev. **C69**, 014903 (2004), [arXiv:hep-ph/0308085].
[34] V. L. Eletsky, M. Belkacem, P. J. Ellis, and J. I. Kapusta, Phys.Rev. **C64**, 035202 (2001), [arXiv:nucl-th/0104029].
[35] C. H. Lee, H. Yamagishi, and I. Zahed, Phys.Rev. **C58**, 2899 (1998), [arXiv:hep-ph/9806391].
[36] J. Ghiglieri, J. Hong, A. Kurkela, E. Lu, G. D. Moore, et al., JHEP **1305**, 010 (2013), [arXiv:hep-ph/1302.5970].
[37] M. Laine, JHEP **1311**, 120 (2013), [arXiv:hep-ph/1310.0164].
[38] I. Ghisoiu and M. Laine, JHEP **10**, 83 (2014), [arXiv:hep-ph/1407.7955].
[39] J. Ghiglieri and G. D. Moore, JHEP **12**, 029 (2014), [arXiv:hep-ph/1410.4203].
[40] B. Schenke and M. Strickland, Phys.Rev. **D76**, 025023 (2007), [arXiv:hep-ph/0611332].
[41] K. Dusling and S. Lin, Nucl.Phys. **A809**, 246 (2008), [arXiv:nucl-th/0803.1262].
[42] G. Gounaris and J. Sakurai, Phys.Rev.Lett. **21**, 244 (1968).
[43] C. D. Roberts and A. G. Williams, Prog.Part.Nucl.Phys. **33**, 477 (1994), [arXiv:hep-ph/9403224].
[44] S. Turbide, Ph. D. Thesis, McGill University (2006).
[45] P. B. Arnold, G. D. Moore, and L. G. Yaffe, JHEP **0111**, 057 (2001), [arXiv:hep-ph/0109064].
[46] G. Vujanovic, J.-F. Paquet, G. S. Denicol, M. Luzum, B. Schenke, et al., Nucl.Phys. **A932**, 230 (2014), [arXiv:hep-ph/1404.3714].
[47] C. Shen, U. Heinz, J.-F. Paquet, and C. Gale, Nucl.Phys. **A932**, 184 (2014), [arXiv:nucl-th/1403.7558].